Full wafer 3D modelling of power distribution during microwave annealing of doped c-Si

S D Das

Centre of Excellence for Green Energy and Sensor Systems,BESU, India

Abstract: *Application of microwave for rapid annealing purposes have been recently introduced for silicon and apart from many advantages that it enjoys, it has also provide avenue to rapid recrystallisation and reduction of defects. One of the applications of such technology is microwave annealed re-crystallised solar cells. In this work, modelling of microwave power spatial distribution in doped crystalline silicon (c-Si) is presented for advancement of re-crystallised solar cell technology. Helmholtz equation was solved for determination of electric field distribution inside the material system using 3D exact Finite Difference Method. Subsequently, microwave power distribution was obtained using application of Poynting power theorem. All results presented in this paper corresponds to Industrial, Scientific and Medical (ISM) frequency of 2.45 GHz.*

Keywords: Microwave, c-Si, annealing, 3D modeling, eFDM

I. INTRODUCTION

Microwave annealing is useful in semiconductor annealing processes because of extremely rapid rise in temperature to very high values. A typical rapid annealing cycle using microwave radiation last for few seconds and could raise the temperature in the range of 2000 ℃ with in fraction of a second depending upon frequency and material [1]. Other advantages of microwave annealing in semiconductor processing includes selective heating, defect elimination in ion implanted silicon, and dopant activation [2-3]. Microwave annealing is a sustainable technology and it is particularly useful for recrystallised solar cells [4]. Large bandgap and narrow bandgap semiconductor processing using microwave annealing has been reported [5-6], but not widely. Dependence of different parameters, such as dimension and composition of sample, mode of incident radiation etc. have been studied in these works.

A full wafer 3D modelling of system will be presented in this work to model the power distribution during microwave annealing. This distribution is responsible for temperature distribution inside a c-Si wafer during microwave annealing which is crucial for uniform recrystallisation for recrystallised solar cells. The distribution pattern depends on standing wave pattern formation of microwave radiation inside the sample. Frequency of microwave along with dimensions of heating chamber and sample, play crucial part in this regard. Magnitude of rise in temperature and its distribution due to absorption of microwave energy also depends on local material properties. In case of narrow bandgap non-polar semiconductor such as c-Si dielectric constant is such material property. Dielectric constant of c-Si depends on may different physical mechanisms and which mechanism will dominate is function of frequency. Thus power distribution is dependent on many different physical parameters and are sensitive to different parameters by different amount. To model the distribution accurately Helmholtz equation needs to be solved with good degree of accuracy. Many different techniques are available for such purpose and one popular method is Finite Difference Method (FDM). Most FDMs introduces truncation errors. A recent technique Exact Finite Difference Method (eFDM) has been introduced in 2D by Wong et. al. (2011), which do not introduce truncation errors [7]. In this work we investigate dependence of absorbed microwave power distribution in doped (c-Si) at ISM frequency of 2.45 GHz at 300K. For such purpose 3D eFDM technique will be introduced first followed by modelling results.

II. THEORY

In non-polar semiconductors such as c-Si the mechanism of absorption at ISM frequency is primarily free-carrier absorption which depends upon doping levels of the material [8]. Power absorbed is calculated using Poynting power theorem [9]. For non-magnetic materials microwave power absorbed in a unit volume is given by [10]:

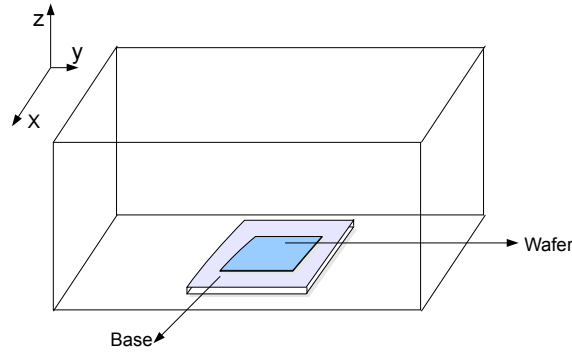$$Q \sim \omega \, \varepsilon_o \varepsilon_c^r |\vec{\xi}|^2 \qquad (1)$$

Fig.1. Schematic of c-Si wafer placed on a microwave transparent plate inside a microwave oven.

where, ε_o is permittivity of free space, ε_c^r is relative imaginary part of complex dielectric function and $\vec{\xi}$ is incident microwave electric field at frequency ω. Electric field distribution of incident microwave radiation inside a material is governed by Maxwell's equations. The electric field distribution in equation (1) is thus obtained by solving Helmholtz equation [10]:

$$\nabla^2\vec{\xi}+\Theta^2\vec{\xi} = 0 \qquad (2)$$

where, $\Theta^2=\omega^2\varepsilon_o\mu_o\varepsilon^r$ is the propagation constant and ε^r is the relative complex dielectric function. In this study we consider a square c-Si wafer placed on a transparent plate inside a microwave oven (Fig. 1). The oven walls are made of metal and hence we consider electric field to be zero at the boundary. Thus for $\xi=f(x,y,z)$ boundary condition can be given by :

$$\xi_{x,y,z=0,L} = 0 \qquad (3)$$

were, L corresponds to maximum values in the direction of x, y and z.

III.   EXACT FINITE DIFFERENCE METHOD

In this section we describe the numerical method for solution of (2). eFDM scheme enables solution to be found numerically without truncation error. The exact FDM scheme is described by Wong et. al and is based on Lambe et. al. method of using weight to modify the central difference operator. Wong et. al. description is for one-dimensional (1D) and two-dimensional (2D) cases. In this work the mathematics is extended to 3D and adopt boundary condition described by (3) instead of radiation boundary condition. The discrete equation corresponding to (2) using Finite Difference Method is:

$$\frac{\xi(x+m,y,z)-2\xi(x,y,z)+\xi(x-m,y,z)}{m^2}+\frac{\xi(x,y+n,z)-2\xi(x,y,z)+\xi(x,y-n,z)}{n^2}$$
$$+\frac{\xi(x,y,z+o)-2\xi(x,y,z)+\xi(x,y,z-o)}{o^2}+\Theta^2\xi=0 \qquad (4)$$

were, standard central difference formula have been used and intervals in x-, y- & z-directions have m, n and o spatial step sizes, respectively. Here, we consider the general case of $m\neq n\neq o$. Using the weight factor W in (4) gives:

$$\frac{\xi(x+m,y,z)+\xi(x-m,y,z)}{m^2}+\frac{\xi(x,y+n,z)+\xi(x,y-n,z)}{n^2}+\frac{\xi(x,y,z+o)+\xi(x,y,z-o)}{o^2}$$
$$-2W\left[\frac{1}{m^2}+\frac{1}{n^2}+\frac{1}{o^2}\right]\xi+\Theta^2\xi=0 \qquad (5)$$

Let $\Theta(x,y,z)=(\theta_1,\theta_2,\theta_3)$ and solution be of the form $\xi=\xi_o e^{i(\theta_1 x+\theta_2 y+\theta_3 z)}$, then (5) gives:

$$\frac{2\cos(\theta_1 m)-W}{m^2}+\frac{2\cos(\theta_2 n)-W}{n^2}+\frac{2\cos(\theta_3 o)-W}{o^2}+\Theta^2=0 \qquad (6)$$

Thus, from (6) the weight factor is obtained as

$$W=\frac{2\left[n^2 o^2\cos(\theta_1 m)+m^2 o^2\cos(\theta_2 n)+m^2 n^2\cos(\theta_3 o)\right]+(mno\,\Theta)^2}{n^2 o^2+m^2 o^2+m^2 n^2} \qquad (7)$$

Using (5) and (7), we can obtain unique solution for electric field $\vec{\xi} = f(x, y, z)$. To establish uniqueness of the solution Uniqueness theorem with proof has been provided below.

Uniqueness Theorem: By using eFDM scheme the Helmholtz equation in 3D

$$\nabla^2 \vec{\xi}(x, y, z) + \Theta^2 \frac{\partial \vec{\xi}(x, y, z)}{\partial t} = 0 \tag{8}$$

with boundary conditions $\xi_{x, y, z = 0, L} = 0$ has a unique solution.

Proof: Let there be two solutions w and v. Also, $u = w - v$ such that it satisfies the equation:

$$\frac{u(x+m, y, z) + u(x-m, y, z)}{m^2} + \frac{u(x, y+n, z) + u(x, y-n, z)}{n^2}$$
$$+ \frac{u(x, y, z+o) + u(x, y, z-o)}{o^2} - 2\omega \left[\frac{1}{m^2} + \frac{1}{n^2} + \frac{1}{o^2} \right] u + \Theta^2 u = 0 \tag{9}$$

which can be written as:

$$\nabla_x^2 u_{ijk} + \nabla_y^2 u_{ijk} + \nabla_z^2 u_{ijk} - 4\omega \left[\frac{1}{m^2} + \frac{1}{n^2} + \frac{1}{o^2} \right] u_{ijk} + \Theta^2 u_{ijk} = 0 \tag{10}$$
$$for\ i = 1, 2, \ldots, m\ ;\ \ j = 1, 2, \ldots n\ ;\ \ k = 1, 2, \ldots o$$

Multiplying (10) by v_{ijk} and summing up over i, j and k, we get

$$\sum_{i, j, k=1}^{m, n, o} \left(\nabla_x^2 u_{ijk} + \nabla_y^2 u_{ijk} + \nabla_z^2 u_{ijk} \right) \bar{v}_{ijk} - \sum_{i, j, k=1}^{m, n, o} \left[4\omega \left(\frac{1}{m^2} + \frac{1}{n^2} + \frac{1}{o^2} \right) + \Theta^2 \right] u_{ijk} \bar{v}_{ijk} = 0 \tag{11}$$

$$for\ i = 1, 2, \ldots, m\ ;\ \ j = 1, 2, \ldots n\ ;\ \ k = 1, 2, \ldots o$$

Using discrete integration by parts,

$$\sum_{i, j, k=1}^{m, n, o} \nabla_x^2 u_{ijk} \bar{v}_{ijk} = \sum_{i, j, k=1}^{m, n, o} \nabla_x u_{ijk} \nabla_x \bar{v}_{ijk} - \frac{1}{m} \sum_{j, k=1}^{n, o} \nabla_x u_{mjk} \bar{v}_{mjk} \tag{12}$$

$$\sum_{i, j, k=1}^{m, n, o} \nabla_y^2 u_{ijk} \bar{v}_{ijk} = \sum_{i, j, k=1}^{m, n, o} \nabla_y u_{ijk} \nabla_y \bar{v}_{ijk} - \frac{1}{n} \sum_{i, k=1}^{m, o} \nabla_y u_{ink} \bar{v}_{ink} \tag{13}$$

$$\sum_{i, j, k=1}^{m, n, o} \nabla_z^2 u_{ijk} \bar{v}_{ijk} = \sum_{i, j, k=1}^{m, n, o} \nabla_z u_{ijk} \nabla_z \bar{v}_{ijk} - \frac{1}{o} \sum_{i, j=1}^{m, n} \nabla_z u_{ijo} \bar{v}_{ijo} \tag{14}$$

along with conditions :

$$\bar{v}_{ijk} = \bar{u}_{ijk} \quad for\ i = 1, 2, \ldots, m\ ;\ \ j = 1, 2, \ldots, n\ ;\ \ k = 1, 2, \ldots, o$$
$$u_{ijk} = 0 \quad for\ i = 0, m\ ;\ \ j = 0, n\ ;\ \ k = 0, o \tag{15}$$

the (11) becomes:

$$\sum_{i, j, k=1}^{m, n, o} \nabla_x u_{ijk} \nabla_x \bar{u}_{ijk} + \sum_{i, j, k=1}^{m, n, o} \nabla_y u_{ijk} \nabla_y \bar{u}_{ijk} + \sum_{i, j, k=1}^{m, n, o} \nabla_z u_{ijk} \nabla_z \bar{u}_{ijk}$$
$$- \sum_{i, j, k=1}^{m, n, o} \left[4\omega \left(\frac{1}{m^2} + \frac{1}{n^2} + \frac{1}{o^2} \right) + \Theta^2 \right] u_{ijk} \bar{u}_{ijk} = 0 \tag{16}$$

Let v_{ijk} be of the form $v_{ijk} = a_1 mi + a_2 nj + a_3 ok + a_4$, then first term in (16) becomes:

$$\sum_{i, j, k=1}^{m, n, o} \nabla_x u_{ijk} \nabla_x \bar{u}_{ijk} = \sum_{i, j, k=1}^{m, n, o} \nabla_x u_{ijk} \nabla_x \left(a_1 mi + a_2 nj + a_3 ok + a_4 \right)$$
$$= a_1 \sum_{i, j, k=1}^{m, n, o} \nabla_x u_{ijk} = a_1 \sum_{j, k=1}^{n, o} \left(u_{mjk} - u_{0jk} \right) = 0 \tag{17}$$

and this is true for ∇_y and ∇_z terms as well in (16). Thus,

$$\sum_{i, j, k=1}^{m, n, o} \left[4\omega \left(\frac{1}{m^2} + \frac{1}{n^2} + \frac{1}{o^2} \right) + \Theta^2 \right] u_{ijk} \bar{u}_{ijk} = 0 \tag{18}$$

Further, since w and q are non zero terms, then for any positive integer *l*,

$$\sum_{i,j,k=1}^{m,n,o} u_{ijk}\,\bar{v}_{ijk}^{l}=0 \tag{19}$$

$$\sum_{i,j,k=1}^{m,n,o} \frac{1}{(l+1)}\nabla_x^2 u_{ijk}\,\bar{v}_{ijk}^{l+1}=0 \tag{20}$$

$$\sum_{i,j,k=1}^{m,n,o} \frac{1}{(l+1)(l+2)}\nabla_x^2 u_{ijk}\,\bar{v}_{ijk}^{l+2}=0 \tag{21}$$

By mathematical induction for $l=1,2,3,...$

$$\sum_{i,j,k=1}^{m,n,o} u_{ijk}\,\bar{v}_{ijk}^{l}=0 \tag{22}$$

Thus, it can be concluded that $u_{ijk}=0$, completing the proof of uniqueness theorem.

IV. RESULTS AND DISCUSSIONS

The spatial distribution of absorbed microwave power inside a metal cavity (microwave oven) was obtained by solving the 3D discrete equation, (5), inside the metal cavity. Full system modeling was carried out by using spatial filtering on 3D matrix, which defines the system. The work was carried out on a 32-bit computer. For implementation the system matrix was converted to vector and an indexing technique defined by:

$$l=I(j-1)+i+(IJ)(k-1), \quad l=1,2,3....IJK \tag{23}$$

was used. Here, i, j and k are indices for x-, y- and z-directions respectively and I, J & K are corresponding maximum values. This approach eliminates nested loop requirement for 3D systems and reduces complexity of the algorithm. Assumption was made that microwave source delivers power which has a spectrum defined by:

$$P(f)=A\exp\left(\frac{f_o-f}{2\sigma^2}\right) \tag{24}$$

Microwave source spectrum vary form instrument to instrument and hence theoretical distribution was considered for quick modeling. However, author considers measured spectrum [9] to be the best source for accurate modeling. The theoretical spectrum defined by (24) is shown in Fig.2, where, f = 2.45 GHz, $\sigma^2=8.86\text{x}10^{10}$ and $A=7.977$ W. The distribution corresponds to 800W of total power. The initial spatial distribution of available power for a given frequency was assumed uniform inside the cavity and the incident flux was obtained using $I=0.5\,c\,\varepsilon_o\,\xi_o^2$.
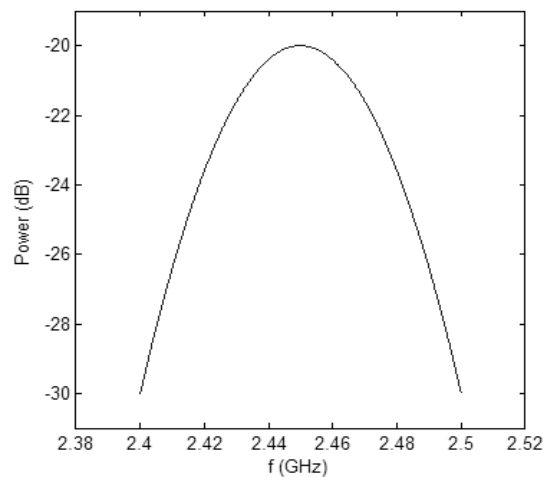

Fig.2 Theoretical power distribution of microwave source.

Microwave power distribution inside an air field cavity with dimensions $28\times29\times20$ cm^3 for different frequencies are shown in Fig. 3. Results include horizontal (Fig. 3 1(a) – 4(a)) and vertical cross sections (Fig. 3 1(b) – 4(b)) of the excited cavity. These results are for 60 iterations with 15 points per wavelength accuracy. The spatial distribution is not same for all frequencies suggesting not all frequencies are well supported by the cavity. Fig.4 provides peak power (P_p) spectrum of the excited cavity, showing for some frequencies power is more concentrated in spatial distribution than others.

For microwave annealing purposes in a multi-mode microwave (such as house hold microwave oven), modeling only sample which is to be heated with appropriate boundary conditions would not produce accurate results of heating distribution inside a sample. Standing wave patterns inside a cavity is guided by the dimensions and properties of the cavity and sample placed inside it [9]. Hence, in this work full system modeling was carried out. A system of dielectric slab placed at the bottom center of the cavity was considered (Fig. 1). Dimensions of the oven cavity was kept as earlier, while dimensions of a slab was $15 \times 15 \times 5$ cm^3. Results of modeling are shown in Fig. 4, for two cases where complex relative dielectric constant ($\varepsilon^r_{c, en}$) of cavity environment is less than complex relative dielectric constant of slab ($\varepsilon^r_{c, slab}$) and $\varepsilon^r_{c, en}$ greater than $\varepsilon^r_{c, slab}$. Clearly, for heating purpose $\varepsilon^r_{c, en} < \varepsilon^r_{c, slab}$ must be maintained, other wise most microwave energy will be concentrated outside the slab. Under this condition sample get heated without heating the ambient. This condition has significant impact on the choice of environment with in the cavity for heating. Choice of environment thus have to be both non-oxidising to the sample and satisfy the above condition for efficient silicon processing. On the other hand for $\varepsilon^r_{c, en} > \varepsilon^r_{c, slab}$ most of microwave energy will be outside the sample. This condition will heat the sample but with less efficiency.
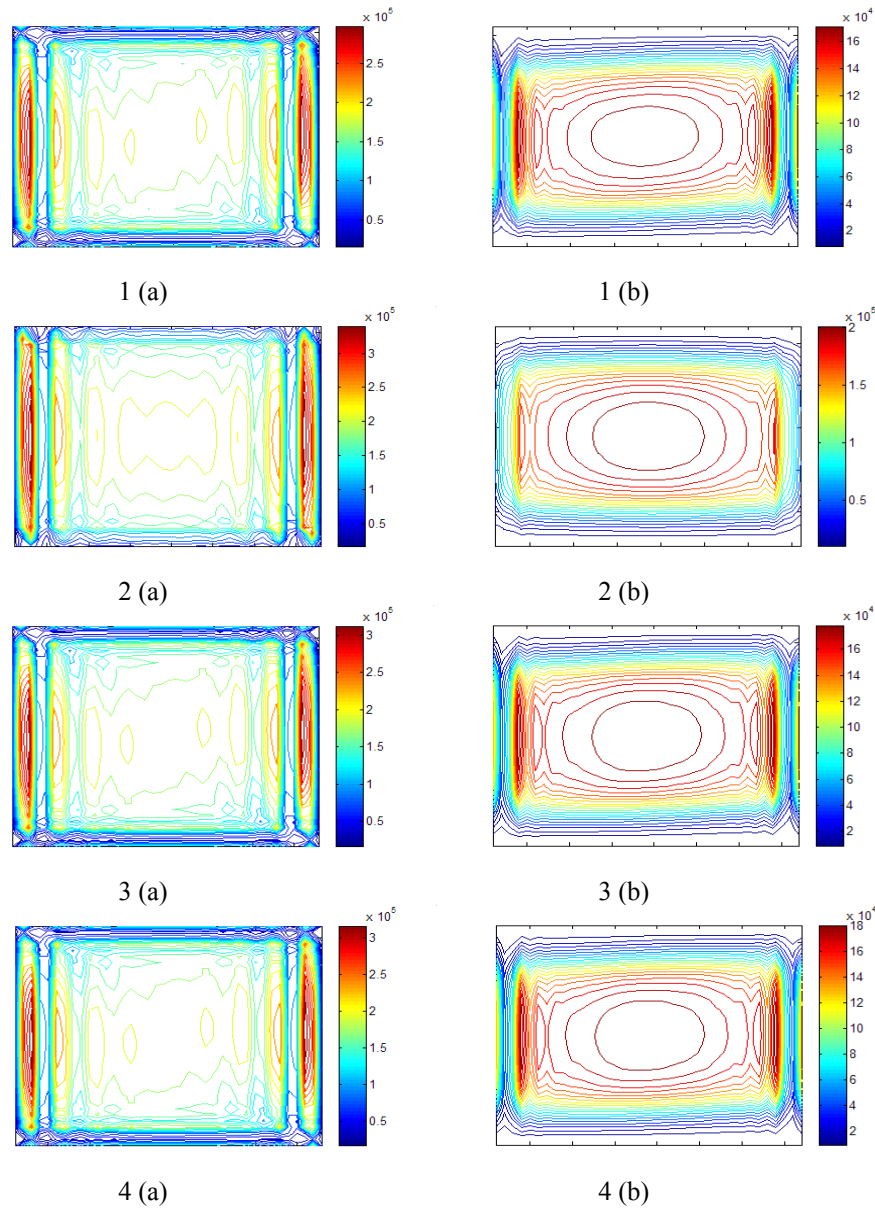

1 (a)   1 (b)

2 (a)   2 (b)

3 (a)   3 (b)

4 (a)   4 (b)

Fig. 3 Microwave power distribution in (a) horizontal and (b) vertical cross section of
an air filled cavity for (1) f = 2.4 GHz, (2) f = 2.45 GHz , (3) f = 2.47 GHz and (4) f = 2.5 GHz.

1 (a)   1 (b)
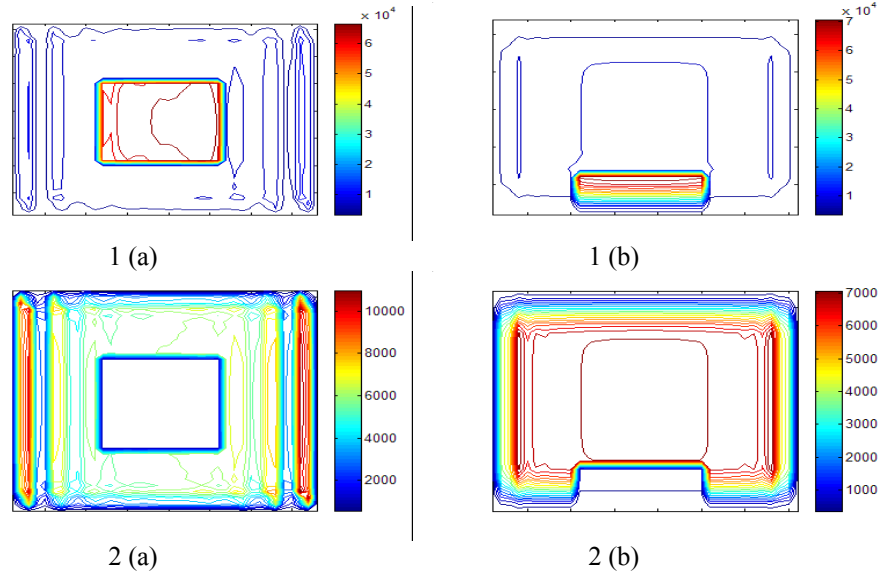

2 (a)   2 (b)

Fig. 4 Absorbed microwave power distribution in (a) horizontal and (b) vertical cross section of

an air filled cavity with a dielectric slab at bottom center at f = 2.4 GHz for (1) $\varepsilon_{c,en}^{r} < \varepsilon_{c,slab}^{r}$
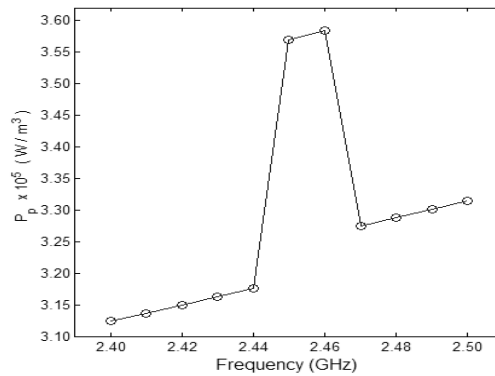
and (2) $\varepsilon_{c,en}^{r} > \varepsilon_{c,slab}^{r}$.

Fig. 5 Peak power (P_p) spectrum of an cavity of dimension 28×29×20 cm^3 filled with air.

From Fig. 5, two frequencies corresponding to highest peak power (f = 2.45GHz) and lowest peak power (f = 2.4 GHz) was chosen and it was found that absorbed power distribution pattern does not vary significantly with frequency with in the sample (Fig.6). This is due to very small difference in peak power values, which is of the order of 0.1 times the peak power values. However, the distribution pattern varies significantly with position of the slab, with dimensions of cavity kept constant. From Fig. 6 and Fig. 7, it is evident patterns inside the sample are significantly influenced by the standing wave patterns due to reflection from cavity walls. Further, dimensions of the sample plays crucial part in distribution pattern as well. Comparing Fig. 6 and Fig. 8, this fact is directly observable. Sample dimensions for Fig. 6 result is 15×15×5 cm^3 while that of Fig. 8 is 15×15×0.6 cm^3. Fig.9 shows variation of power distribution with input total power. The distribution is not significantly influenced by the input power. However, amplitude of the peak power is dependent on the total input power and thus total input power will be significant for controlling temperature inside the sample.

The complex dielectric function ε for c-Si is dependent on free-carrier absorption and is given by Drude's model [8, 11]:

$$\varepsilon = \varepsilon_r + i\,\varepsilon_c = \varepsilon_{core} + \frac{4\pi i}{\omega}\left[\frac{n_e e^2 \tau_e}{m_e(1-i\,\omega\,\tau_e)} + \frac{n_h e^2 \tau_h}{m_h(1-i\,\omega\,\tau_h)}\right] \qquad (25)$$

For n-type c-Si with, suffix 'e' stands for majority carrier electron while suffix 'h' stands for minority carrier hole. In (25), n is free-carrier concentration, m is effective mass and τ is relaxation time constant. Fig. 10 shows dependence of imaginary part of dielectric function (ε_c) on doping density (N$_D$) at 300K. The doping species for this case is phosphorous. At 300K, power absorption distribution from full system modeling of air filled cavity with a c-Si wafer (10.5×10.5×0.06 cm^3 and N$_D$ = 1x10^{20} cm^3) on borosilicate glass slab (15×15×0.6

cm³) at bottom center is shown in Fig. 11. The simulation was carried out with 15x15x1000 points per wavelength. Fig. 12 shows results for similar conditions as Fig. 11 but with wafer orientation changed from horizontal flat position to vertical upright position. With vertical up right position the power distribution inside the wafer is significantly non uniform as compared to horizontal flat position.
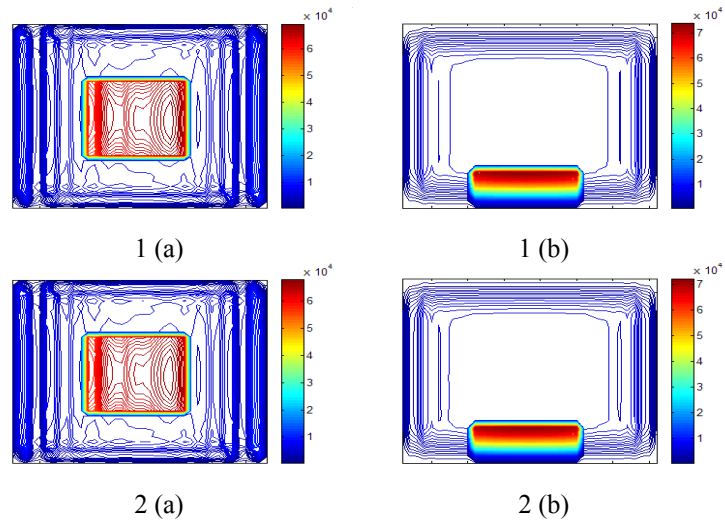

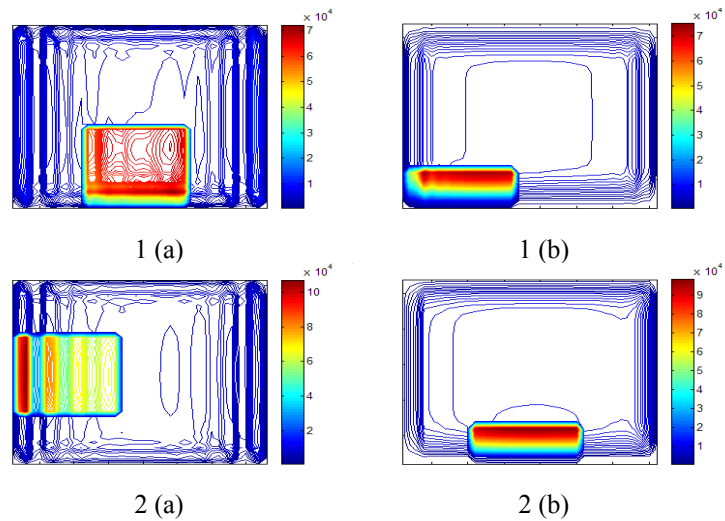1 (a)   1 (b)

2 (a)   2 (b)

Fig. 6 Absorbed microwave power distribution in (a) horizontal and (b) vertical cross section of an air filled cavity with a dielectric slab at bottom center at (1) f = 2.45 GHz and (2) f = 2.4 GHz .

1 (a)   1 (b)

2 (a)   2 (b)

Fig. 7 Absorbed microwave power distribution in (a) horizontal and (b) vertical cross section of an air filled cavity with a dielectric slab at (1) bottom front and (2) bottom left. f = 2.45 GHz.
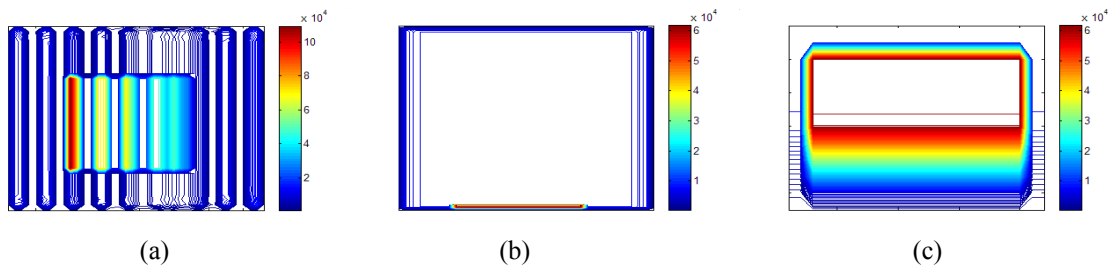

(a)   (b)   (c)

Fig. 8 Absorbed microwave power distribution in (a) horizontal, (b) vertical cross sections of an air filled cavity with a dielectric slab (15×15×0.6 cm³) at bottom center. (c) zoomed in vertical cross section of slab. f = 2.45 GHz.

(a)   (b)   (c)
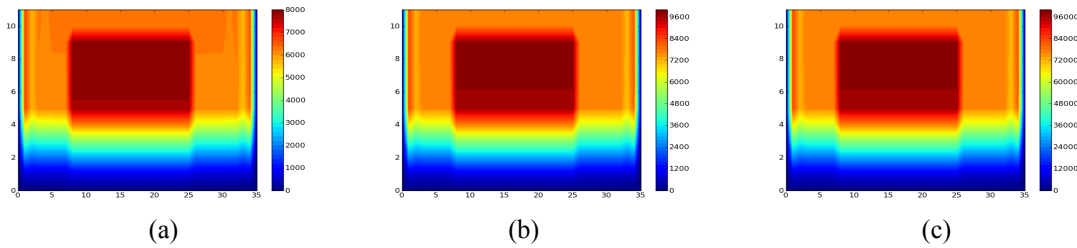
Fig. 9 Absorbed microwave power distribution in an air filled cavity with a dielectric slab
($15 \times 15 \times 5$ cm^3) at bottom center. Total input power (a) 800 W, (b) 1000 W and (c) 10,000 W.
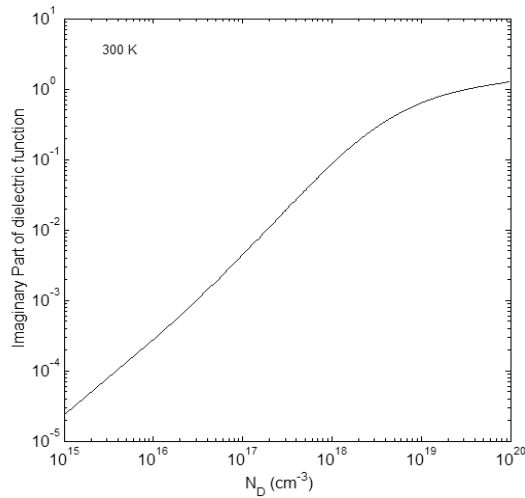All the figures show zoomed results. f = 2.45 GHz.

Fig. 10 Dependence of imaginary part of dielectric function (ε_c) on donor
density (N_D) for c-Si at 300K.

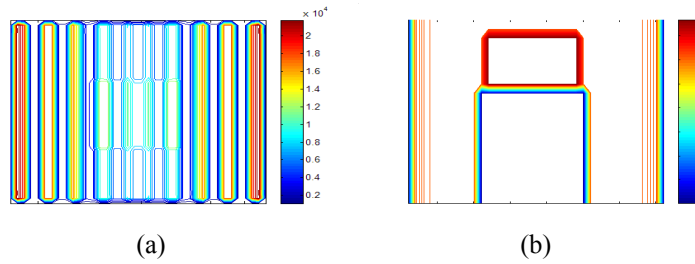(a)   (b)

Fig. 11 Absorbed microwave power distribution in an air filled cavity with a c-Si wafer on
borosilicate glass slab at bottom center. (a) Horizontal and (b) vertical (zoomed) cross sections. f = 2.45 GHz.

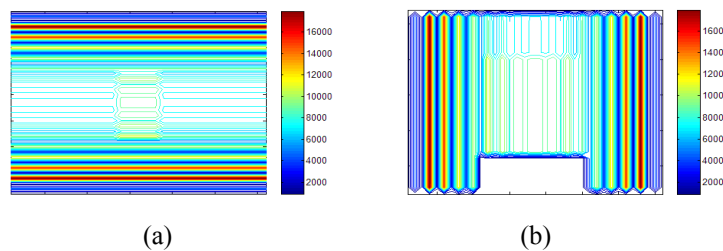
(a)   (b)

Fig. 12 Absorbed microwave power distribution in an air filled cavity with a c-Si wafer on
borosilicate glass slab at bottom center with wafer in vertical position. (a) Horizontal (zoomed)
and (b) vertical cross sections. f = 2.45 GHz..

V. CONCLUSION

In conclusion, 3D modeling results for microwave power distribution in phosphorous doped c-Si wafer has been presented for ISM frequency of 2.45 GHz at 300K. A new 3D modeling technique, eFDM, has been introduced for such purpose which has no truncation error. Results from modeling show inefficient power distribution with in the sample for rectangular cavity (house hold microwave oven). This shows cavity shape and dimension needs to be redesigned to make the annealing process efficient and uniform for re-crystallized solar cell work.

Acknowledgments

REFERENCES

[1] M. V. Rao, Ultra-fast Microwave Heating for Large Bandgap Semiconductor Processing, *Advances in Induction and Microwave Heating of Minerals & Organic Materials* ISBN:978-953-307-522-8, 2011, 459.

[2] R. N. P. Vemuri, M. J. Garde, N. D. Theodore, and T. L. Alford, Dopant Activation in Arsenic -Implanted Si by Susceptor-Assisted Low-Temperture Microwave Anneal, *IEEE Electron Device Letters 32* , 2011, 1122-1124.

[3] S. C. Fong, C. Y. Wang, T. H. Chang, and T. S. Chin, Crystallization of amorphous Si film by microwave annealing with SiC susceptors, *Applied Physics Letters 94*, 2009, 102104.

[4] S. D. Das, Prospects of Microwave Heating in Silicon Solar Cell Fabrication – A Review, *IOSR-JEEE, 6(3)*, 2013, 28-38.

[5] J. N. Lee, Y. W. Choi, B. J. Lee and B. T. Ahn, Microwave-induced low-temperature crystallization of amorphous silicon thin films, *Journal of Applied Physics, 82(6),* 1997, 2918-2921.

[6] Md. R. Hossan, D-Y Byun, P. Dutta, Analysis of microwave heating for cylindrical shaped objects, *International Journal of Heat and Mass Transfer*, *53,* 2010, 5129–5138.

[7] Y. S. Wong and G. Li, Exact Finite Difference Schemes For Solving Helmholtz Equation At Any Wavenumber, *International J. of Numerical Analysis and Modelling, Series B, 2 (1)*, 2011, 91-108.

[8] D. C. Dibben, *Numerical and Experimental Modelling of Microwave applicators* (University of Cambridge, 1995).

[9] A. K. Shukla, A. Mondal and A. Upadhyay, Numerical Modelling of Microwave Heating, *Science of Sintering, 42,* 2010, 99.

[10] T Basak, Role of lateral and radial irradiations on efficient microwave processing of food cylinders, *Chemical Engineering Science, 62,* 2007, 3185 – 3196.

[11] T. Sameshima, H. Hayasaka and T. Haba, Analysis of Microwave Absorption Caused by Free Carriers in Silicon, *Japanese Journal of Applied Physics, 48,* 2009, 021204.